

Active responsive colloids driven by intrinsic dichotomous noiseNils Göth ¹, Upayan Baul,¹ and Joachim Dzubiella^{1,2,*}¹*Applied Theoretical Physics–Computational Physics, Physikalisches Institut, Albert-Ludwigs-Universität Freiburg, D-79104 Freiburg, Germany*²*Cluster of Excellence livMatS @ FIT–Freiburg Center for Interactive Materials and Bioinspired Technologies, Albert-Ludwigs-Universität Freiburg, D-79110 Freiburg, Germany*

(Received 27 July 2022; accepted 28 November 2022; published 22 December 2022)

We study the influence of intrinsic noise on the structure and dynamics of responsive colloids (RCs), which actively change their size and mutual interactions. The colloidal size is explicitly resolved in our RC model as an internal degree of freedom (DOF) in addition to the particle translation. A Hertzian pair potential between the RCs leads to repulsion and shrinking of the particles, resulting in an explicit responsiveness of the system to self-crowding. To render the colloids active, their size is internally driven by a dichotomous noise, randomly switching (“breathing”) between growing and shrinking states with a predefined rate, as motivated by recent experiments on synthetic active colloids. The polydispersity of this dichotomous active responsive colloid (D-ARC) model can be tuned by the parameters of the noise. Utilizing stochastic computer simulations, we study crowding effects on the spatial distributions, relaxation times, and self-diffusion of dense suspensions of the D-ARCs. We find a substantial influence of the “built-in” intrinsic noise on the system’s behavior, in particular, transitions from unimodal to bimodal size distributions for an increasing colloid density as well as intrinsic noise-modified diffusive translational dynamics. We conclude that controlling the noise of internal DOFs of a macromolecule or cell is a powerful tool for active colloidal materials to enable autonomous changes in the system’s collective structure and dynamics towards the adaptation of macroscopic properties to external perturbations.

DOI: [10.1103/PhysRevE.106.064611](https://doi.org/10.1103/PhysRevE.106.064611)**I. INTRODUCTION**

For the development of soft functional materials, scientists are typically inspired by proven concepts in nature, as expressed by bacteria, cells, and microswimmers [1,2]. Unlike inert matter, such as wool or plastic, they all have a power source, such as ATP or glucose, which is consumed. And they all have something enginelike built in that enables an internally controlled change of their appearance or movement. Consequently, their overall behavior and motion are not purely a result of external forces but partially driven by internal mechanisms. Thus, it is not a surprise that active particles have become a large field of interest. The treated topics range from motile Brownian particles [3–5] over particles with autonomously oscillating size [6–8] to active (nonmotile) hydrogels with pH-feedback [9].

To construct livinglike materials, internal activity has to be linked with a large responsiveness to stimuli in the environment [10]. For example, bacteria use quorum sensing, emitting and detecting small molecules to evaluate local density, to adapt their internal (genetic, size, speed, etc.) behavior according to their population [11,12]. Inspired from nature, the approved strategies of responsiveness have been transferred to create artificial materials with controlled response. Widely investigated are, for example, thermosensitive

poly(*N*-isopropylacrylamide) (PNIPAM) microgels, which possess a volume phase transition (switching between collapsed and swollen states) upon small changes in temperature [13], and other stimuli, such as ionic strength [14], pH [7,15,16], or light [17]. Potential applications are, e.g., target-oriented drug-delivery where colloids can carry and eject a drug at the diseased tissue [18,19], or stimuli-responsive switchable catalysis [20,21].

Responsiveness, switching, and internal activity lead to nonequilibrium distributions and fluctuations on the particle scale, eventually coupled to their collective structure and function. For instance, some bacteria switch randomly between a normal and a persistence state and are therefore resistant to antibiotic treatment due to a small amount of bacteria in the persistence state [22,23]. In synthetic systems, block copolymer vesicles show a controlled contraction and expansion behavior upon applying environmental triggers [24,25]. Thereby, a stochastic “breathing” akin to dichotomous noise behavior may be realized. But also autonomously self-pulsating colloids can exhibit irregularities and dichotomous-noise-like effects in their oscillations [26]. In biology, control of internal processes by intrinsic noise gives cells the opportunity to engender heterogeneity in a colony and thereby gain robustness or efficiency [27]. However, these are only a few of the many examples of stochastic or pseudostochastic effects in biology and chemistry [28,29].

Theoretically, it is crucial that fluctuations and noise are well defined in a model; in particular, in equilibrium the

*Corresponding author: joachim.dzubiella@physik.uni-freiburg.de

fluctuation-dissipation theorem must hold [30]. Fluctuations and noise are used to coarse-grain one or multiple microscopic effects that are computationally too expensive to simulate in detail. The Gaussian noise for the translational coordinates typically coarse-grains the interaction with the surrounding solvent (“bath”) with a random walk. The fluctuations of active internal degrees of freedom (DOFs) may be far from being Gaussian (white), and we can speak of nonequilibrium and colored noise effects [31]. A simple option to violate fluctuation-dissipation and include a kind of activity is to couple different DOFs to different thermostats [32–36], where one could picture the internal “engine” as an additional heat bath that can cool or heat the internal DOF. Another possibility is that the particles switch randomly between different kinds of states. This can be an active switching between different sizes [37,38], between attractive and repulsive particle-particle interactions [39], or between different motility states [40].

In this work, we study the effects of intrinsic dichotomous noise in a model of responsive colloids (RCs) on colloidal structure and dynamics. We recently developed an RC model that resolves besides the translational DOFs an additional internal DOF (or “property”) [41], for example, one representing the colloid’s size [42,43]. The property is assumed to be governed by stochastic dynamics enabling temporal changes and responses to neighboring colloids and other environmental stimuli. The idea of an additional DOF has been used with increasing frequency in recent years to model complex colloids [44–48] or proteins [49]. Other than in previous works [35,42], we do not drive the internal DOF with a Gaussian noise but rather with a dichotomous noise. This means that each colloid switches randomly between a growing and a shrinking state. In contrast to known, more coarse-grained and phenomenological models of active switching colloids [37,39], this model is based on a microscopic Hamiltonian, and it includes also the continuous transition between the two states. The dichotomous noise is one of the simplest switching noises (relevant for the experimental examples above), and it has the advantage of being a very well-studied noise [4,50–56]. In particular, it has a known analytical solution for the harmonic potential [56]. Using this dichotomous model in stochastic, overdamped simulations, we study intrinsic noise effects on the structure and dynamics of dense colloidal dispersions in the steady state. For an enhanced physical interpretation of the results, we also insert a recapitulation of the existing single-particle solution [56], and we present a modified perturbation theory for RCs [43].

II. MODEL AND METHODS

A. Dichotomous active responsive colloid model

To model suspensions of active responsive colloids (ARCs), we utilize our previously introduced RC model [42] as a basis, and we modify it with respect to the type of noise for the internal DOF. Consider N colloids with translational temperature T , where each colloid (particle) i has a center-of-mass position in three-dimensional (3D) space \mathbf{x}_i . Additionally, each colloid has an associated property σ_i , in our case study representing a sphere’s diameter. This leaves

us with in total $4N$ DOFs in the system (three translational and one internal DOF per particle).

For our free energy, we consider a single-particle term $U(\sigma)$ and a pair potential term ϕ . Together we obtain the Hamiltonian

$$H = \frac{1}{2} \sum_i \sum_{j \neq i} \phi(r_{ij}, \sigma_i, \sigma_j) + \sum_i U(\sigma_i), \quad (1)$$

where $r_{ij} = |\mathbf{x}_i - \mathbf{x}_j|$ is the pair distance between two particles i and j .

An appropriate pair potential for soft repulsive and elastic colloids, such as hydrogel particles, is the Hertzian potential [57,58]. The Hertzian interaction potential of two particles is

$$\phi_{ij} = \phi(r_{ij}; \sigma_i, \sigma_j) = \epsilon \left(1 - \frac{r_{ij}}{\tilde{\sigma}}\right)^{5/2} \Theta\left(1 - \frac{r_{ij}}{\tilde{\sigma}}\right) \quad (2)$$

with the average diameter of both particles $\tilde{\sigma} = (\sigma_i + \sigma_j)/2$ and $\Theta(\cdot)$ denoting the Heaviside-step function. The potential strength is set to $\epsilon = 500 k_B T$, which is found for typical thermosensitive colloids in experiments [57]. The pair potential is purely repulsive and cut at $\tilde{\sigma}$. Thus, not overlapping particles do not interact, and the larger the overlap, the higher the potential energy. A more detailed discussion about the Hertzian potential can be found elsewhere [42,57].

In addition to the pair potential, RCs feature the internal parent energy landscape, $U(\sigma)$, for the evolution of the size property σ . We choose U to be a harmonic potential of the form $U(\sigma) = \frac{1}{2\beta\delta^2}(\sigma - \sigma_0)^2$ with a potential width of $\delta = 0.2\sigma_0$, and $\beta = 1/k_B T$ being the inverse thermal energy. This defines a preferred particle size of σ_0 and avoids very small and very large particle sizes due to its confinement. A Gaussian parent implies a simple linear elastic response of the size, while for hydrogels more accurate nonlinear responses can also be straightforwardly employed [47].

The translational force \mathbf{F}_i^T acting on a particle i is given by the gradient of the Hamiltonian in Eq. (1). We transfer this procedure to the property coordinate σ , which leads to the forces

$$\mathbf{F}_i^T = -\nabla_i H = -\sum_{j \neq i} \nabla_i \phi_{ij}, \quad (3)$$

$$F_i^\sigma = -\partial_{\sigma,i} H = -\partial_{\sigma,i} U - \sum_{j \neq i} \partial_{\sigma,i} \phi_{ij}, \quad (4)$$

where ∇_i and $\partial_{\sigma,i}$ are the derivatives with respect to the translational coordinates and the property coordinate, respectively. Since the pair potential ϕ_{ij} also affects the property, an overlap of two particles leads not only to a repulsion but also to a shrinking of both particles [42]. Thus, the particles respond internally to their local environment.

Regarding the equations of motions, as in [42] we neglect the inertia term for the viscous and stochastic motion of all DOFs of the RCs, leading to overdamped Langevin-like dynamics. To solve the stochastic differential equations, we chose the basic Euler algorithm, which is computationally slower but simpler compared to more sophisticated methods like the Runge-Kutta or Milstein scheme [59]. The discretized

functions $f(\sigma)$ and $g(\sigma)$:

$$p(\sigma) = p_0 \frac{g(\sigma)}{v_D^2 g^2(\sigma) - f^2(\sigma)} \times \exp \left[2\lambda \int^{\sigma} d\sigma' \frac{f(\sigma')}{v_D^2 g^2(\sigma') - f^2(\sigma')} \right] \quad (10)$$

with a normalization factor p_0 . By inserting our $f(\sigma)$ and $g(\sigma)$ from Eq. (9) into Eq. (10), we obtain for the stationary probability distribution [56]

$$p(\sigma) = \begin{cases} p_0 \left(1 - \left(\frac{\sigma - \sigma_0}{\Delta} \right)^2 \right)^\alpha, & \sigma \in (\sigma_0 - \Delta, \sigma_0 + \Delta), \\ 0 & \text{otherwise} \end{cases}$$

$$\text{with } \Delta = v_D \beta \gamma_\sigma \delta^2, \quad \alpha = \lambda \beta \gamma_\sigma \delta^2 - 1 \quad (11)$$

and $p_0 = \Gamma(\alpha + 3/2) / [\sqrt{\pi} \Gamma(\alpha + 1)]$ being a prefactor normalizing the distribution to 1 which contains the gamma function Γ . The parameter Δ defines the width of the distribution, which is only nonzero in the interval $\sigma \in (\sigma_0 - \Delta, \sigma_0 + \Delta)$. At both boundaries, the force due to the single-particle potential and the dichotomous force cancel. Consequently, the particles have a minimum and a maximum size, which is identical to the distribution's boundaries. The dichotomous velocity v_D is proportional to the width Δ . The second parameter describing the property distribution is the exponent α , which depends on the switching rate λ of the noise.

The property distribution for different values of α can be seen in Fig. 1(b). In the limit of no switching ($\lambda \rightarrow 0$, $\alpha \rightarrow -1$), the distribution consists of two Dirac δ -functions, one at each boundary, which is a simple bidisperse system. For low switching rates ($\alpha < 0$), the DOF develops a probability distribution with two finite-width peaks and a lower probability in between, which is a bimodal distribution. The transition state to unimodality (one peak) is a uniform distribution ($\alpha = 0$). Further rise of the switching rate ($\alpha > 0$) results in an increasingly sharp peak in the center. In the limit of infinitely fast switching ($\lambda \rightarrow \infty$, $\alpha \rightarrow \infty$) we obtain one Dirac δ -function at σ_0 , characterizing a monodisperse system. Gaussian white noise is obtained in the limit $\lambda \rightarrow \infty$, $v_D \rightarrow \infty$ with $\lambda/v_D^2 = \beta \gamma_\sigma/2$.

Already the single-particle solution is interesting from a physical point of view of (bio)chemical matter. It enables colloids or bacteria to control their own size distribution by *internally* tuning their switching rate (and swelling velocity), which is important for function [60]. We focus in this work on the influence of the switching rate λ , which is an important parameter for biological systems, like bacteria, to regulate switching between different phenotypes [23]. However, note that the control of the parameter v_D would also be quite powerful since it is in the LDL directly proportional to the distribution width.

Beyond the LDL, at higher densities, particles interact and the distribution $p(\sigma)$ will be modified. We thus distinguish in our work between the property distribution in the LDL $p(\sigma)$ (the ‘‘parent’’) and the *emergent* property distribution for nonvanishing particle densities, $N(\sigma)$.

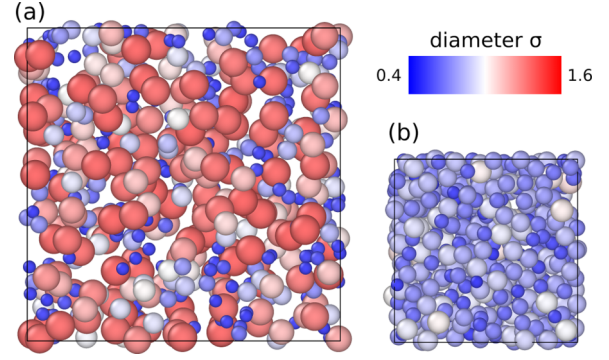


FIG. 2. Snapshots of the simulation. (a) Low particle density ($\rho\sigma_0^3 = 0.19$) and low switching rate ($\lambda\tau = 0.01$). (b) High particle density ($\rho\sigma_0^3 = 0.95$) and high switching rate ($\lambda\tau = 0.1$). The box with periodic boundary conditions is depicted by thin black lines. The particle's color visualizes its size; red indicates a large particle, blue a small one, and a white particle has a size of $\sigma = \sigma_0$. The two boxes are scaled to the same reference length; the left box has a side length of $L \approx 14\sigma_0$ and the right box has a side length of $L \approx 8\sigma_0$, respectively. Snapshots are made with OVITO [64].

D. Simulation details

The computer simulations leading to the numerical results contain $N = 512$ particles in a cubic box with periodic boundary conditions. To obtain a certain particle number density ρ , the length of the box is fixed to $L = \sqrt[3]{N/\rho}$. Simulation snapshots for two different densities are shown in Fig. 2. Initially all particles are distributed on a simple cubic lattice filling in the whole box. Simultaneously, each particle receives a random state [(+) or (-)] and a size σ_i pulled from a Gaussian distribution centered at σ_0 and with variance δ^2 .

For the time evolution, a simple Euler algorithm is used [cf. Eqs. (5) and (6)]. The duration of one time step is $\Delta t = 10^{-4}\tau$. Each simulation contains 3×10^6 (or 5×10^6) equilibration steps to ensure that the system is in the steady state, and 10^7 subsequent production steps, which are used to collect data. The configuration is written out every 1000th time step. For each analyzed parameter set, five independent simulations were performed; all results are averages over these five data sets. With $\gamma_\sigma = 1000\gamma_\tau$ and a dichotomous velocity of $v_D = 0.01\sigma_0/\tau$, the property motion is much slower than the translational motion. This choice leads to internal relaxations much slower than translation, which is motivated by small, chemically stimulated microgels for which translational diffusion happens much faster than size changes due to the complex internal processes [61]. It is also known in general that internal degrees of freedom can slow down internal relaxation beyond idealized hydrodynamic conformational behavior, for example in the slowing down of polymer folding rates due to internal friction processes [62]. All model and simulation parameters are summarized in Table I.

To implement the dichotomous noise, we make use of method 2 presented in [54]. Each particle gets initially a random remaining time $t_r = -\ln(u)/\lambda$, where u is drawn from a uniform distribution between 0 and 1. After the remaining time is over, the particle switches its state and a new remaining time, drawn in the same way, is assigned to the particle. This procedure leads to the same noise as deciding at each time

TABLE I. Parameters in the numerical simulation, their values, and their description. The table is divided into four parts: unit sizes, model parameters, varied parameters, and simulation-specific parameters.

Parameter	Value	Description
σ_0	1	unit length and mean size of an isolated particle
τ	1	unit time defined by translational diffusion $D_T^0 = 1 \sigma_0^2 / \tau$
β	1	inverse unit energy ($k_B T = 1/\beta$)
δ	$0.2\sigma_0$	width of $U(\sigma)$
γ_T^0	$1 \tau / (\beta \sigma_0^2)$	translational friction coefficient of a particle with size σ_0
γ_σ	$10^3 \tau / (\beta \sigma_0^2)$	property friction coefficient
v_D	$0.01 \sigma_0 / \tau$	dichotomous velocity
$\beta \epsilon$	500	Hertzian potential strength
$\lambda \tau$	{0.01, 0.025, 0.032, 0.05, 0.1, 0.25}	(dichotomous) switching rate
$\rho \sigma_0^3$	{0.019, 0.19, 0.57, 0.95, 1.33}	number density of particles
N	512	number of particles
Δt	$10^{-4} \tau$	length of one time step
	$300\tau - 500\tau$	equilibration time
	1000τ	production time
	$10/\tau$	output frequency

step whether a particle switches its state or not, but it saves some computational time.

The used random number generator for a uniform distribution between 0 and 1 is the Mersenne Twister MT19937, followed by the Marsaglia polar method [63] to obtain random numbers drawn from a Gaussian distribution.

E. Radial distribution function and structure factor

A common measure to analyze the structure of a suspension is the radial distribution function (RDF), $g(r)$. It correlates the pair distances between particles and is defined as [30]

$$g(r) = \frac{1}{4\pi r^2 \rho N(N-1)} \left\langle \sum_i \sum_{j \neq i} \delta(r - r_{ij}) \right\rangle \quad (12)$$

with $r_{ij} = |\mathbf{x}_i - \mathbf{x}_j|$. Since we can split our particles into two groups [(+)- and (-)-state particles], we can also split the RDF into its components via

$$g(r) = \frac{1}{4} g_-(r) + \frac{1}{4} g_+(r) + \frac{1}{2} g_\pm(r), \quad (13)$$

where $g_-(r)$ and $g_+(r)$ are the RDFs of only the (-)- and (+)-state particles, respectively. Meanwhile, $g_\pm(r)$ includes only distances of particles with different states. We also calculate the structure factor [65]

$$S(q) = 1 + 4\pi \rho \int_0^\infty dr r^2 \frac{\sin(qr)}{qr} [g(r) - 1], \quad (14)$$

which can be obtained by scattering experiments [30].

F. Diffusion coefficient

For characterizing the translational diffusion in our systems, we compute the spatial mean-squared displacement (MSD)

$$\text{MSD}(t) \equiv \langle [\mathbf{x}(t) - \mathbf{x}(0)]^2 \rangle. \quad (15)$$

For long times, the MSD is proportional to t and we can obtain an effective diffusion coefficient through fitting via $\text{MSD}(t) =$

$6D_T^{\text{eff}} t$. Only the values within the interval $t \in [10\tau, 250\tau]$ are used for the fit to omit the short-time diffusion and the MSD values with small statistics in the case for long times.

G. Property autocorrelation function

A common measure to access the dynamics and relaxation times of a DOF is the autocorrelation function (ACF). We define the normalized ACF of the property as

$$C_{\sigma\sigma}(t) = \frac{\langle \sigma(t)\sigma(0) \rangle - \langle \sigma \rangle^2}{\langle \sigma^2 \rangle - \langle \sigma \rangle^2}, \quad (16)$$

which starts at $C_{\sigma\sigma}(t=0) = 1$ and converges to 0 in the long-time limit because the initial and final values of σ are uncorrelated due to the random processes. The ACF for one dichotomous particle in a harmonic potential, which corresponds to our LDL, can be determined analytically [56] and reads

$$C_{\sigma\sigma}^{\text{LDL}}(t) = \frac{1}{t_\delta - t_D} [t_\delta e^{-t/t_\delta} - t_D e^{-t/t_D}] \quad (17)$$

with the time constants $t_\delta = \beta \gamma_\sigma \delta^2$ and $t_D = 1/2\lambda$. We see that the normalized ACF is a sum of two independent exponential decays. The potential time t_δ describes the timescale on which a noiseless particle moves to the center of the single-particle potential. The dichotomous time t_D characterizes the timescale of the mean lifetime of a state. Both processes are independent of each other. Finally, to quantify the decay's speed we use the correlation time t_{corr} , which is defined by

$$C_{\sigma\sigma}(t_{\text{corr}}) = 1/e. \quad (18)$$

In equilibrium systems, the time derivative of the unnormalized autocorrelation function is proportional to the response function (fluctuation-dissipation theorem) [55]. This relation was already successfully used in nonequilibrium systems [66], which gives us access to a utilizable response function.

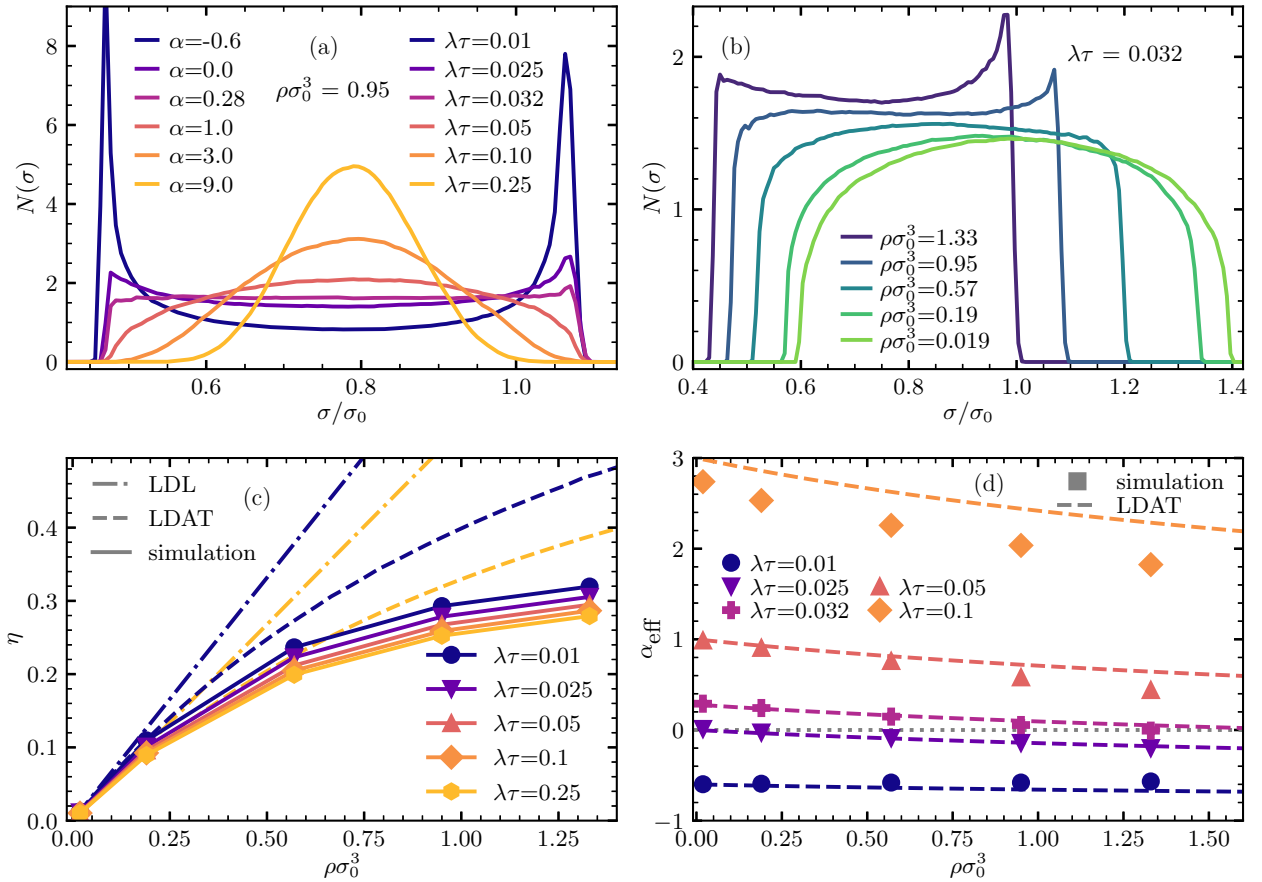


FIG. 3. (a) Emergent property distribution $N(\sigma)$ for a density of $\rho\sigma_0^3 = 0.95$ and different switching rates. The displayed α denote the exponent in the LDL which can be converted to λ using Eq. (11). The values close to the edges are impaired by the binning algorithm, and they have to be treated with caution. (b) Property distribution $N(\sigma)$ for a constant switching rate and different particle densities. One can see a transition from unimodal to bimodal for increasing densities. (c) Packing fraction $\eta = \pi\rho\langle\sigma^3\rangle/6$ vs number density for different switching rates. The symbols and solid lines depict the simulation results, the dashed lines the LDAT, and the dash-dotted line the linear scaled LDL. (d) The symbols depict the effective exponent α_{eff} from fitting Eq. (11) to the obtained property distribution. The dashed lines show again the prediction from the LDAT.

III. RESULTS

A. Property distribution

We first examine property distributions for nondilute particle densities: In Fig. 3(a) the emergent property distribution $N(\sigma)$ is shown for $\rho\sigma_0^3 = 0.95$ and different switching rates. Although the system is quite dense, we can see clear similarities to the low-density limit (LDL). The edges of the bimodal distributions are still very sharp because of the comparatively slow movement in the σ -dimension. Consequently, a particle's σ -movement can be seen as in a mean potential established by the other particles in addition to the single-particle potential. However, an interesting phenomenon can be extracted from the $\alpha = 0$ distribution in Fig. 3(a), which corresponds to the uniform distribution in the LDL [cf. Fig. 1(b)]. The increase in density shifts the flat distribution towards bimodality. This can more clearly be seen in Fig. 3(b), which shows also the property distribution but only for $\lambda\tau = 0.032$ and different densities in return. Four points shall be stressed from this figure: (i) For increasing density, the distribution's center shifts to lower values of σ [cf. snapshot in Fig. 2(b)], while (ii) the distribution gets narrower at the same time. Both (i) and (ii)

are also observed in [42], where a Gaussian noise is used for the property instead of the dichotomous noise. (iii) The distribution makes a transition from unimodality to bimodality. While it is unimodal for this specific λ for low densities (e.g., $\rho\sigma_0^3 = 0.019$), it is bimodal for higher densities (e.g., $\rho\sigma_0^3 = 1.33$). Thus, it is a density-induced transition. (iv) We observe asymmetries for higher densities. For $\rho\sigma_0^3 = 0.95$, one can see that the right edge shows an indication of bimodality while the left edge has a unimodal shape. Figure 3(a) shows that these asymmetries are comparatively small for the covered densities.

The crowding effect itself is well described with the mean packing fraction $\eta = \pi\rho\langle\sigma^3\rangle/6$, which is the volume fraction filled by the colloids. The packing fraction is shown in Fig. 3(c) versus number density. The simulation results of our RCs show a sublinear behavior of $\eta(\rho)$ due to the colloid shrinking in crowded environments [42]. The spread with respect to the switching rate results from the different property distribution shapes: low switching rates privilege extreme sizes, while a small and a large colloid fill more space than two average-sized colloids (σ^3 -dependency). Therefore, η increases with decreasing $\lambda\tau$. We complement our result

with a perturbation theory for RCs [42]. Briefly, we make a low-density assumption and calculate the mean force on a particle with size σ . By a perturbation of the free-energy landscape $U(\sigma)$ with nonzero particle densities, we obtain our low-density approximation theory (LDAT). Details and equations are shown in Appendix. Predictions from our LDAT for the packing fraction can be seen as dashed lines in Fig. 3(c). Even though the theory underestimates the crowding effect for high densities, it exhibits sublinear behavior, which is the crucial point.

As we saw in Fig. 3(a), the property distribution's shape for higher densities is still quite similar to that in the LDL described by Eq. (11). Therefore, we want to fit Eq. (11) to the obtained distribution and determine an effective value for α , which then describes the distribution's shape and the degree of unimodality/bimodality. The left and right edge of a distribution are identified by taking the first σ_f and last value σ_1 of the normalized distribution [$\int d\sigma N(\sigma) = 1$] crossing $N(\sigma) = 0.001$. With these parameters, the new center $\sigma_1 = (\sigma_f + \sigma_1)/2$ and width $\Delta_1 = (\sigma_1 - \sigma_f)/2$ of the distribution can be calculated. Equation (11) with given σ_1 and Δ_1 can now be fitted to the obtained distribution with α as the fit parameter. The emerged value is the effective exponent α_{eff} . Figure 3(d) shows α_{eff} as a function of density for different switching rates. We see for all covered switching rates a decrease of α_{eff} for rising ρ . This illustrates the observed transition from unimodality ($\alpha_{\text{eff}} > 0$) to bimodality ($\alpha_{\text{eff}} < 0$).

The basis for the uni-to-bimodal transition lies in the mean potential seen by a particle. In the LDL we have for the property only the quadratic single-particle potential. The additional potential, arising from particle-particle interactions, shifts the total potential to lower σ values and narrows it. While the dichotomous velocity remains unmodified, the distance between minimum and maximum σ shortens. Hence, more particles gather at the distribution's edges, which induces a trend to bimodality. This bimodality is not a consequence of barrier crossing in the free-energy landscape as in our previous RC model [43], but is a result of the underlying noise as in [31,66]. The LDAT (see Appendix) can now be used to approximate the property distribution for nonvanishing densities. The α_{eff} predicted from the LDAT is also shown in Fig. 3(c). It describes the trend quite well for low densities, and it also predicts the density-induced transition. For higher densities, the LDAT underestimates the transition, which is a result of the neglect of higher-order interaction terms in the theory.

Regarding the physical interpretation of our results, we speculate that the observed density behavior may enable active colloidal suspensions to perform a collective response to changes in density without communication via chemical signaling. This could be interesting in combination with autonomously, self-oscillating particles where the occurrence of the oscillations can be highly dependent on the density and numbers of neighboring "coupling" particles [7]. The unimodal-bimodal transition may also engender automatic changes in size diversity depending on the density. This could be an important factor in the development of adaptive materials [60] based on synthetic active colloidal dispersions.

B. RDF and structure factor

We now analyze the spatial particle-particle correlations by inspecting radial distribution functions (RDFs). Figure 4(a) shows the RDFs for $\rho\sigma_0^3 = 0.95$ and different switching rates. The observed behavior for high $\lambda\tau$ is as expected for common monodisperse liquids [67]. However, for $\lambda\tau = 0.01$ we observe a clear deviation, consisting of a substructure of three washed-out step functions. The explanation can be found when splitting the RDF into its individual components [cf. Eq. (13)], as is done in Fig. 4(b). If we consider only the (−)-state particles in our system (green dashed line), we spot a peak that is located at $r_p \approx 0.7\sigma_0$; this is much lower than the peak of the total $g(r)$ ($r_p \approx 1.0\sigma_0$). The reason is that (−)-state particles are in general much smaller than the average. The same can be said for (+)-state particles (violet dashed line) with the difference that the peak is at further distances. Only $g_{\pm}(r)$ shows an approximately "normal" behavior with a peak in between the others. Since the three peaks have a comparably large distance and the total RDF is the sum of these three [$g_{\pm}(r)$ counts double], $g(r)$ shows a substructure. Thus, the appearance of the substructure is not a result of the particles' dynamics but simply of the bimodal property distribution. Note that a substructure is present for all switching rates, but is in general not visible in the RDF due to too close peaks.

To visualize the substructure, we plot the corresponding structure factor [see Eq. (14)] of Fig. 4(a) in Fig. 4(c). For all $\lambda\tau$ we see a first peak at $q\sigma_0/2\pi \approx 1.2$ resulting from the presence of the first coordination shell. The second peak shows the substructure: while it is clearly visible for high switching rates, it is suppressed for $\lambda\tau = 0.01$. A similar but weaker effect is also visible for $\lambda\tau = 0.025$, where the second minimum is suppressed. The approximately identical behavior for $q\sigma_0/2\pi < 1$ for all $\lambda\tau$ implies a very similar long-range order while losing short-range structure ($q\sigma_0/2\pi > 1$) is recognized for high $\lambda\tau$. This can be explained by the broad property distribution, which leads to many different occurring short particle-particle distances [see also Fig. 4(a)].

We tentatively conclude that physically the intrinsic noise and internal distributions have a major global effect and can serve as control mechanisms to tune the collective structure of the colloid dispersion.

C. Transition times of internal states

We now turn to the system's property dynamics. For this, we utilize the normalized ACF $C_{\sigma\sigma}(t)$ introduced in Eq. (16). In Fig. 5(a) it is shown for $\rho\sigma_0^3$ and different switching rates. We can see that the higher $\lambda\tau$ is, the faster the correlation decays. This can be explained by the LDL solution in Eq. (17): The property relaxes slower for lower switching rates because drastic changes of the property only appear after a switch. In addition, we can see that the ACF converges for a high $\lambda\tau$ (yellow line) to a simple exponential decay, because the dichotomous time constant $t_D = 1/2\lambda$ decreases and provides a negligible term in Eq. (17). The large fluctuations for high switching rates arise because the initial $\langle\sigma^2\rangle$ and final value $\langle\sigma\rangle^2$ are very similar for narrow property distributions. To rationalize our findings, we show in Fig. 5(a) also the theoretical ACF calculated from the perturbation theory. It is obtained by inserting the new potential width δ_1 from the

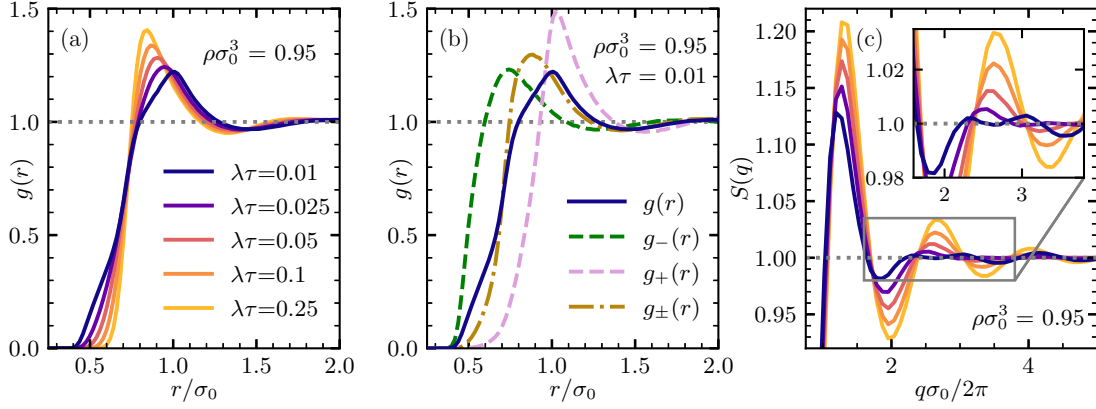


FIG. 4. (a) RDF for a number density of $\rho\sigma_0^3 = 0.95$ and different switching rates. (b) The $g(r)$ can be split into its components according to Eq. (13). The dashed blue line shows the total RDF, the green (violet) dashed line shows the $g(r)$ of only the $(-)$ -state [$(+)$ -state] particles; $g_{\pm}(r)$ (golden dash-dotted line) is for RDF between particles of different states. (c) Structure factor calculated from the RDFs shown in (a) with the same colors as in (a).

LDAT (see Appendix) into Eq. (17). We find a surprisingly good agreement with the simulation, which can be traced back to the dominant influence of $\lambda\tau$ in Eq. (17) compared to the small changes in δ_1 .

The obtained correlation times are shown in Fig. 5(b) as a function of $\lambda\tau$ for different $\rho\sigma_0^3$. The correlation time decreases with increasing $\lambda\tau$; this is true for all covered number

densities. In addition, we see that t_{corr} decreases also with increasing number density because for larger $\rho\sigma_0^3$ the distribution's width gets narrower (cf. Fig. 3). Since the intrinsic time constant, t_{δ} , in Eq. (17) is proportional to the potential's width squared, this leads to an effective larger time constant, yielding a faster decay. Figure 5(b) also shows as a gray dash-dotted line the theoretical t_{corr} from the ACF in the LDL [cf. Eq. (17)]. This coincides with the obtained simulation results for low densities (light green circles).

Hence, our results demonstrate how the internal dynamics of colloids are partially controlled by the intrinsic noise. However, to get full control, supervision of the free energy landscape is also necessary.

D. Translational diffusion

Finally, we analyze the translational diffusive dynamics. Figure 6(a) demonstrates that the MSD in our system is proportional in time and thus normal diffusive. Figure 6(b) shows the effective diffusion coefficient D_T^{eff}/D_T^0 versus $\rho\sigma_0^3$ for different switching rates, where D_T^0 denotes the diffusion coefficient of an isolated particle with size σ_0 . The diffusion shows two qualitatively different regimes: For densities up to $\rho\sigma_0^3 \approx 0.9$ the effective diffusion coefficient decreases. This can be explained by crowding, which slows diffusion down. The crowding is poorly characterized by the number density because the average particle size shrinks in our model with $\rho\sigma_0^3$. Therefore, crowding is better described by the packing fraction η displaying a saturating behavior [cf. Fig. 3(c)]. As a consequence, for high densities the shrinking particle sizes lead to a higher Stokes diffusion. This also explains the differences for various switching rates: In the LDL, the effective diffusion coefficient is proportional to $\langle 1/\sigma \rangle$, which increases for more bimodal distributions (lower α). This is in contrast to existing simulation results of a bidisperse model with switching between a small and a large size [38]. The crucial difference is that changes in the switching rate in [38] do not change the size distribution.

In summary, the effective diffusion coefficient is comparatively constant under changes in density if one considers that two completely different physical effects (increased crowding

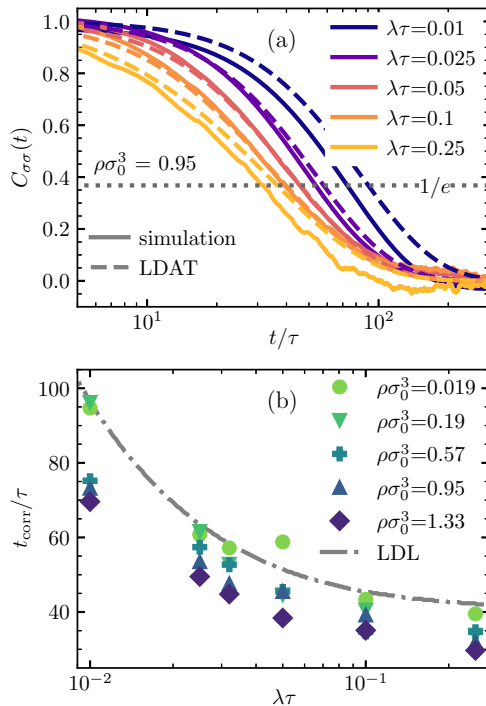


FIG. 5. (a) Normalized ACF of the property [see Eq. (16)] for a number density of $\rho\sigma_0^3 = 0.95$ and different switching rates. The solid lines belong to the simulation results, while the dashed lines show the theoretical prediction by Eq. (17) with a new potential width δ_1 . Intersections with the gray dotted line at $C_{\sigma\sigma} = 1/e$ yield the correlation times. (b) Correlation time t_{corr} from Eq. (18) as a function of λ for different $\rho\sigma_0^3$. The gray dash-dotted line indicates the theoretical solution in the LDL of Eq. (17).

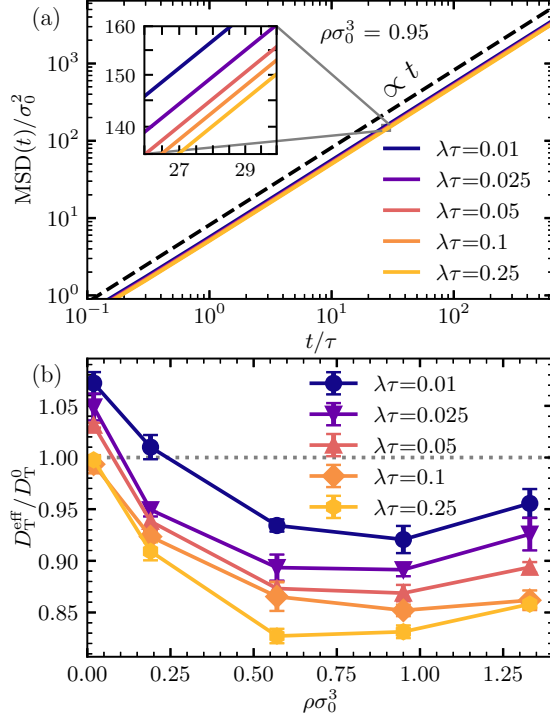


FIG. 6. (a) MSD as a function of time according to Eq. (15) for a high density ($\rho\sigma_0^3 = 0.95$) and different switching rates. The black dashed line shows the slope for a proportionality to time in this log-log plot. (b) Effective diffusion coefficient vs density for different switching rates. The normalization is done with respect to the diffusion of a free particle with size σ_0 , D_T^0 .

and decreased Stokes friction) work against each other. For a specific pair potential, it might even be possible to achieve a density-independent effective diffusion coefficient. This could be an interesting mechanism for the transport of colloids to keep them mobile at higher densities. The results in this section demonstrate that it is possible to control the translational diffusive dynamics by tuning collectively the internal switching rate.

E. Effective temperature definition

In this section, we attempt to define an effective temperature of the property to facilitate an interpretation of the system on a thermodynamic level. This is inspired by already existing approaches to effective temperature definitions in nonequilibrium, e.g., for active motile Brownian particles [5] and two-temperature-baths systems [32–35]. In our system, the translational movement has an intrinsic temperature T as the input parameter fed into the Gaussian noise; this is not the case for the dichotomous noise. Choosing a standard calculation via the property’s mean-squared velocity is not possible since velocities are not considered in an overdamped system. However, the options of defining such a temperature are nonetheless manifold, and several of them are discussed in the recent work by Medeiros and Queirós [55]. For simplicity, we consider here an isolated particle to evade the interaction term. Other definitions also include interactions but only for white noise [32].

TABLE II. Limits of the definitions of the dichotomous temperature T_D [cf. Eq. (19)] and the property temperature T_σ [cf. Eq. (20)]. The analyzed limits are the white-noise limit as well as the limits for high and low switching rates.

Limit	T_D	T_σ
$v_D, \lambda \rightarrow \infty, \lambda/v_D^2 = \gamma_\sigma/(2T)$	$\rightarrow T$	$\rightarrow T$
$\lambda \rightarrow \infty$	$\rightarrow 0$	$\rightarrow 0$
$\lambda \rightarrow 0$	$\rightarrow \infty$	$\rightarrow T(\Delta/\delta)^2$

For our system, we predefine two requirements for a proper temperature: First, in the Gaussian white-noise limit [$\lambda, v_D \rightarrow \infty$ with $\lambda/v_D^2 = \gamma_\sigma/(2T)$] the defined temperature has to converge to the translational temperature T , since this describes the thermodynamic equilibrium case. Second, in the no-noise limit ($\lambda \rightarrow \infty$ and $v_D = \text{const}$), representing a frozen property DOF, the temperature has to be zero. In the following, we will present and discuss two possible temperature definitions.

The MSD of a free particle in one dimension driven only by dichotomous noise is known [4] and for long times and finite switching rates linear in time. With the resulting diffusion coefficient $D_D = v_D^2/2\lambda$ and the Stokes-Einstein equation $D = k_B T/\gamma$ it is possible to define a dichotomous temperature

$$T_D = \frac{\gamma_\sigma v_D^2}{2\lambda k_B} = T \frac{(\Delta/\delta)^2}{2\alpha + 2}. \quad (19)$$

This *Ansatz* via the effective diffusion coefficient can also be applied to active Brownian particles [5]. The limits of Eq. (19) are shown in Table II and fulfill both of our requirements, namely the Gaussian white-noise limit and the no-noise limit. The term *dichotomous temperature* refers to the fact that this temperature definition is only noise-dependent and does not include the free-energy landscape.

Another possible definition was introduced in [55] by comparing definitions from kinetic theory, system entropy, and response theory. In the overdamped case, they consistently result in the same temperature, for us the *property temperature* [68],

$$T_\sigma = \frac{\beta\delta^2 v_D^2 \gamma_\sigma^2 / k_B}{1 + 2\beta\delta^2 \gamma_\sigma \lambda} = T \frac{(\Delta/\delta)^2}{2\alpha + 3}. \quad (20)$$

It indeed defines a proper temperature that fulfills both of our requirements (see Table II). It is worth mentioning that this temperature definition obeys the fluctuation-dissipation relation between the response function $R(t, t')$ and the unnormalized autocorrelation function $\partial \tilde{C}_{\sigma\sigma}(t, t')/\partial t' = TR(t, t')$, which holds in thermal equilibrium [55].

Both definitions predict a qualitative trend for the distributions, which is known for temperatures: For low temperatures, the probability distribution in a confined potential is narrow [cf. $\alpha = 9.0$ in Fig. 1(b)]. With increasing temperature, the probability distribution gets broader. In the limit of no switching ($\lambda \rightarrow 0, v_D = \text{const}$), the interpretations of the two temperatures are more difficult. The term “noise” is also questionable because it is a constant term. While the dichotomous temperature T_D diverges, the property temperature

converges to $T(\Delta/\delta)^2$. Nonetheless, the property σ in our system does not even change in time in this limit, so a vanishing temperature could also be justified. However, the permanent energy supply of the internal noise to maintain the size feels conflictive with a cold temperature. Also, the diffusion never reaches proportionality $\text{MSD} \propto t$ for long times. In a nutshell, is there even a reasonable temperature for the low switching rate limit?

We introduced two effective temperature definitions to describe our additional property degree of freedom, namely the dichotomous temperature T_D and the property temperature T_σ . The definitions, although from completely different *Ansätze*, are very similar [see Eqs. (19) and (20)]. But which one is better? This question cannot be answered. Both definitions have their justification. The dichotomous temperature characterizes the activity of the noise while the property temperature describes the property motion in the harmonic potential. Both definitions fulfill the requirements of the Gaussian white-noise limit ($T_i \rightarrow T$) and the convergence towards zero in the high switching rate limit. At the same time, both definitions yield strange results in the low switching rate limit, both in different ways.

The discussion shows that a reasonable temperature definition of a system with dichotomous noise is difficult and can be controversial. Nonetheless, an effective temperature definition gives us the possibility to compare it to the translational temperature and to have an effective parameter to describe qualitative trends.

IV. CONCLUSION

In summary, we have introduced and characterized a model for (nonmotile) active responsive colloids (ARCs) by assuming that non-Gaussian dichotomous noise governs the internal fluctuations of the particles. This leads to the dichotomous ARC (D-ARC) model.

The intrinsic noise is controlled by a dichotomous velocity and an internal switching rate, leading already for a single-particle with a harmonic confinement of the internal DOF to nontrivial parent distributions and dynamic unimodal-bimodal transitions. We emphasize that these transitions, first having a purely mathematical nature, have already interesting consequences when interpreted in a physicochemical context. They enable “living” colloidal particles to control their own size distribution by internally tuning their switching rate and swelling velocity for a possible adaptation of function [60]. The switching rate is indeed an important parameter for biological systems, like bacteria, to regulate transitions between different phenotypes [23]. In addition, we demonstrate in particular that the modification of intrinsic noise (which an active particle can do) has substantial physical effects on the collective behavior of the dispersion:

(i) The intrinsic noise parameters (swelling/shrinking velocity and switching rate) induce a transition from unimodal to bimodal behavior, significantly controlling single-particle behavior.

(ii) The noise-controlled property distribution and its transition is modified by packing and crowding; in turn, the collective liquid structure and dynamics is affected and tuned, and property distributions are self-consistently modified.

(iii) Diffusion is homeostatic in the compressible RCs; it can be actively tuned by the intrinsic noise and is relatively constant over the tested density range.

Hence, as a key message of this paper, the type of internal fluctuations can play a substantial role not only for single particles but also for the structure and dynamics of the whole interacting dispersion. The main ingredient of the dichotomous noise leading to the observed behavior is the temporary persistence in the direction of motion. We expect other noises with this characteristic to show qualitatively similar results. Examples in two dimensions are active Brownian particles or the parental active model [31]. We demonstrated a similarly striking behavior already for a simpler model of ARCs where the internal DOF was coupled to a different temperature bath (while still with white noise) than the translation [35]. In contrast to the latter work, however, introducing a colored noise with more “control buttons” showed much more complexity because of the richer internal structure—including a uni- to bimodal transition—and the dynamics of a single particle.

An interesting study for the future could be the coupling of the individual (particle-dependent) noise and the internal DOF, leading to feedback. This could lead to collective oscillations of existing self-oscillating colloids [26] or other synchronous behavior as they happen in bacteria [12]. The following question, therefore, automatically arises: How can the “decision” of a single particle lead to collective changes by chemical signaling? This is another proven concept in bacterial and animal kingdoms.

ACKNOWLEDGMENTS

We thank Michael Bley, Polina Gaidrik, and Sebastian Milster for useful discussions. J.D. acknowledges support by the state of Baden-Württemberg through bwHPC and the German Research Foundation (DFG) through Grant No. INST 39/963-1 FUGG (bw-ForCluster NEMO) and by the DFG via Grant No. WO 2410/2-1 within the framework of the Research Unit FOR 5099 “Reducing Complexity of Nonequilibrium Systems.”

APPENDIX: PERTURBATION THEORY IN THE LOW-DENSITY APPROXIMATION

We attempt to compare the simulation results to a theoretical prediction. Therefore, we calculate observables within a simple low-density approximation theory (LDAT), which essentially is a perturbation approach for the free energy starting from the LDL. We start with the pair-property distribution function $g(r; \sigma, \sigma')$, which is the conditional probability for a particle with size σ to find a particle with size σ' at a distance r . By approximating that this pair-property distribution function is given by the LDL expression, we obtain [41]

$$g(r; \sigma, \sigma') \approx \exp[-\beta\phi(r; \sigma, \sigma')]. \quad (\text{A1})$$

This is an equilibrium assumption that we apply to our out-of-equilibrium system. We will see that our system is in a quasiequilibrium, making this a reasonable approach for low densities. To obtain the radial distribution function out of the σ -resolved $g(r; \sigma, \sigma')$, one has to integrate out the properties

σ and σ' [41],

$$g(r) = \int d\sigma \int d\sigma' N(\sigma) N(\sigma') g(r; \sigma, \sigma'), \quad (\text{A2})$$

where $N(\sigma)$ is the emergent property distribution.

The aim of our perturbation theory is to approximate this emergent distribution, since many observables can be calculated or approximated with it (e.g., RDF, packing fraction, size ACF). The *Ansatz* we choose is identical to the one used in [43], however we have to modify it at some point. The mean force on a particle with property σ originating from interactions with other particles is given as

$$F_{\text{pp}}(\sigma) = -\rho \int_V d^3r \int_{-\infty}^{\infty} d\sigma' N(\sigma') \frac{\partial \phi(r; \sigma, \sigma')}{\partial \sigma} g(r; \sigma, \sigma'). \quad (\text{A3})$$

This is the force $-\partial\phi/\partial\sigma$ between two particles with sizes σ, σ' and distance r , where the variables r and σ' are integrated out. As shown in [43], by applying the LDL [Eq. (A1)], Eq. (A3) can be written as

$$F_{\text{pp}}(\sigma) = -\frac{5}{4}\pi\rho\epsilon\kappa[\sigma^2 + 2\sigma\langle\sigma\rangle + \langle\sigma^2\rangle] \quad (\text{A4})$$

with $\kappa \approx 6.377 \times 10^{-4}$ for $\beta\epsilon = 500$, and $\langle\cdots\rangle$ denoting the ensemble average with respect to the emergent distribution.

The discontinuity of the parent distribution at the boundaries $\sigma_0 \pm \Delta$ makes the further procedure as in [43] unreasonable for our system. Therefore, we choose a numerical approach to obtain the emergent distribution. We assume that the disturbed property distribution can still be described by Eq. (11) but with a new center σ_1 , a new width Δ_1 , a new

exponent α_1 , and within a harmonic potential with new width δ_1 . This *Ansatz* requires a quadratic energy landscape. To be self-consistent, we therefore linearize Eq. (A4) by doing a first-order Taylor expansion around σ_1 of the quadratic term $\sigma^2 \approx 2\sigma_1\sigma - \sigma_1^2$. This results in a quadratic term for the interparticle free-energy term $\mathcal{F}_{\text{pp}}(\sigma) = -\int_0^\sigma d\sigma' F_{\text{pp}}(\sigma')$. By inserting the expectation values of the emergent distribution

$$\langle\sigma\rangle = \sigma_1 \quad \text{and} \quad \langle\sigma^2\rangle = \sigma_1^2 + \frac{\Delta_1^2}{2\alpha_1 + 3} \quad (\text{A5})$$

into Eq. (A4), we obtain a function with only two unknowns (σ_1, Δ_1). The initially free parameters $\delta_1 = \delta/\sqrt{1 + 5\pi\rho\beta\epsilon\kappa\delta^2\sigma_1}$ and $\alpha_1 = \frac{\lambda\Delta_1}{v_D} - 1$ can be eliminated by the definition of the new quadratic potential and the relations in Eq. (11), respectively. Together with the linear single-particle force term $F_{\text{sp}} = -\partial_\sigma U(\sigma)$, we get the total mean force $F_{\text{tot}} = F_{\text{sp}} + F_{\text{pp}}$. The latter has to fulfill again the two boundary conditions

$$F_{\text{tot}}(\sigma_1 - \Delta_1) = v_D \quad \text{and} \quad F_{\text{tot}}(\sigma_1 + \Delta_1) = -v_D, \quad (\text{A6})$$

because sizes outside these boundaries are not possible in the steady state. We can solve the two equations in (A6) numerically for σ_1 and Δ_1 for different particle densities ρ and therefore obtain a LDAT for $N(\sigma; \rho)$.

The general theoretical approach is quite universal and can easily be adapted to other interaction potentials, noises, and single-particle potentials [43]. The dependence of Eq. (A4) on the potential strength and the hard-sphere limit are discussed in [43].

-
- [1] B. C. Buddingh and J. C. M. van Hest, *Acc. Chem. Res.* **50**, 769 (2017).
- [2] H.-W. Huang, M. S. Sakar, A. J. Petruska, S. Pané, and B. J. Nelson, *Nat. Commun.* **7**, 12263 (2016).
- [3] T. F. F. Farage, P. Krinninger, and J. M. Brader, *Phys. Rev. E* **91**, 042310 (2015).
- [4] P. Romanczuk, M. Bär, W. Ebeling, B. Lindner, and L. Schimansky-Geier, *Eur. Phys. J.: Spec. Top.* **202**, 1 (2012).
- [5] C. Bechinger, R. Di Leonardo, H. Löwen, C. Reichhardt, G. Volpe, and G. Volpe, *Rev. Mod. Phys.* **88**, 045006 (2016).
- [6] T. Masuda, A. M. Akimoto, M. Furusawa, R. Tamate, K. Nagase, T. Okano, and R. Yoshida, *Langmuir* **34**, 1673 (2018).
- [7] D. J. Bell, D. Felder, W. G. von Westarp, and M. Wessling, *Soft Matter* **17**, 592 (2021).
- [8] E. Tjhung and L. Berthier, *Phys. Rev. E* **96**, 050601(R) (2017).
- [9] I. Maity, C. Sharma, F. Lossada, and A. Walther, *Angew. Chem., Int. Ed.* **60**, 22537 (2021).
- [10] A. Walther, *Adv. Mater.* **32**, 1905111 (2020).
- [11] M. B. Miller and B. L. Bassler, *Annu. Rev. Microbiol.* **55**, 165 (2001).
- [12] L. Wang, D. Fan, W. Chen, and E. M. Terentjev, *Sci. Rep.* **5**, 15159 (2015).
- [13] Y. Lu and M. Ballauff, *Prog. Polym. Sci.* **36**, 767 (2011).
- [14] F. A. Plamper and W. Richtering, *Acc. Chem. Res.* **50**, 131 (2017).
- [15] J. Heckel, S. Loescher, R. T. Mathers, and A. Walther, *Angew. Chem., Int. Ed.* **60**, 7117 (2021).
- [16] R. Cruz-Silva, L. Arizmendi, M. Del-Angel, and J. Romero-Garcia, *Langmuir* **23**, 8 (2007).
- [17] G. Pasparakis and M. Vamvakaki, *Polym. Chem.* **2**, 1234 (2011).
- [18] S. R. Abulateefeh, S. G. Spain, J. W. Aylott, W. C. Chan, M. C. Garnett, and C. Alexander, *Macromol. Biosci.* **11**, 1722 (2011).
- [19] M. A. C. Stuart *et al.*, *Nat. Mater.* **9**, 101 (2010).
- [20] R. Roa, S. Angioletti-Uberti, Y. Lu, J. Dzubiella, F. Piazza, and M. Ballauff, *Z. Phys. Chem.* **232**, 773 (2018).
- [21] M. Kanduć, W. K. Kim, R. Roa, and J. Dzubiella, *Mol. Syst. Des. Eng.* **5**, 602 (2020).
- [22] N. Q. Balaban, *et al.*, *Nat. Rev. Microbiol.* **17**, 441 (2019).
- [23] D. Dubnau and R. Losick, *Mol. Microbiol.* **61**, 564 (2006).
- [24] B. Yan, D. Han, O. Boissière, P. Ayotte, and Y. Zhao, *Soft Matter* **9**, 2011 (2013).
- [25] S. Lin, J. Shang, X. Zhang, and P. Theato, *Macromol. Rapid Commun.* **39**, 1700313 (2018).
- [26] T. Narita, H. Takakura, N. Ogata, H. Kawakita, and Y. Oishi, *Chem. Commun.* **49**, 919 (2013).
- [27] M. B. Elowitz, A. J. Levine, E. D. Siggia, and P. S. Swain, *Science* **297**, 1183 (2002).
- [28] M. Dittrich and E. Snejdrova, *J. Pharm. Sci.* **103**, 3560 (2014).
- [29] P. C. Bressloff, *J. Phys. A* **50**, 13 (2017).

- [30] J.-L. Barrat and J.-P. Hansen, *Basic Concepts for Simple and Complex Liquids* (Cambridge University Press, Cambridge, 2003).
- [31] L. Caprini, A. R. Sprenger, H. Löwen, and R. Wittmann, *J. Chem. Phys.* **156**, 071102 (2022).
- [32] A. Y. Grosberg and J.-F. Joanny, *Phys. Rev. E* **92**, 032118 (2015).
- [33] V. Dotsenko, A. Maciołek, O. Vasilyev, and G. Oshanin, *Phys. Rev. E* **87**, 062130 (2013).
- [34] R. R. Netz, *Phys. Rev. E* **101**, 022120 (2020).
- [35] P. Gaindrik, U. Baul, and J. Dzubiella, *Phys. Rev. E* **106**, 014613 (2022).
- [36] J. Smrek, I. Chubak, C. N. Likos, and K. Kremer, *Nat. Commun.* **11**, 26 (2020).
- [37] M. Bley, J. Dzubiella, and A. Moncho-Jordá, *Soft Matter* **17**, 7682 (2021).
- [38] M. Bley, P. I. Hurtado, J. Dzubiella, and A. Moncho-Jordá, *Soft Matter* **18**, 397 (2022).
- [39] H. Alston, A. O. Parry, R. Voituriez, and T. Bertrand, *Phys. Rev. E* **106**, 034603 (2022).
- [40] A. Sabri, X. Xu, D. Krapf, and M. Weiss, *Phys. Rev. Lett.* **125**, 058101 (2020).
- [41] Y.-C. Lin, B. Rotenberg, and J. Dzubiella, *Phys. Rev. E* **102**, 042602 (2020).
- [42] U. Baul and J. Dzubiella, *J. Phys.: Condens. Matter* **33**, 174002 (2021).
- [43] U. Baul, N. Göth, M. Bley, and J. Dzubiella, *J. Chem. Phys.* **155**, 244902 (2021).
- [44] G. Kapteijns, W. Ji, C. Brito, M. Wyart, and E. Lerner, *Phys. Rev. E* **99**, 012106 (2019).
- [45] L. Berthier, E. Flenner, C. J. Fullerton, C. Scalliet, and M. Singh, *J. Stat. Mech.* (2019) 064004.
- [46] S. Ciarella, M. Rey, J. Harrer, N. Holstein, M. Ickler, H. Löwen, N. Vogel, and L. M. C. Janssen, *Langmuir* **37**, 5364 (2021).
- [47] A. Scotti, A. R. Denton, M. Brugnoli, J. E. Houston, R. Schweins, I. I. Potemkin, and W. Richtering, *Macromolecules* **52**, 3995 (2019).
- [48] M. Urich and A. R. Denton, *Soft Matter* **12**, 9086 (2016).
- [49] J. Stegen and P. van der Schoot, *Soft Matter* **11**, 2036 (2015).
- [50] K. Kitahara, W. Horsthemke, and R. Lefever, *Phys. Lett. A* **70**, 377 (1979).
- [51] C. Van Den Broeck, *J. Stat. Phys.* **31**, 467 (1983).
- [52] A. Morita, *Phys. Rev. A* **41**, 754 (1990).
- [53] J. Masoliver, *Phys. Rev. A* **45**, 706 (1992).
- [54] C. Kim, E. K. Lee, and P. Talkner, *Phys. Rev. E* **73**, 026101 (2006).
- [55] J. R. Medeiros and S. M. D. Queirós, *J. Stat. Mech.* (2021) 063205.
- [56] J. M. Sancho, *J. Math. Phys.* **25**, 354 (1984).
- [57] D. Paloli, P. S. Mohanty, J. J. Crassous, E. Zaccarelli, and P. Schurtenberger, *Soft Matter* **9**, 3000 (2013).
- [58] L. Rovigatti, N. Gnan, L. Tavagnacco, A. J. Moreno, and E. Zaccarelli, *Soft Matter* **15**, 1108 (2019).
- [59] P. E. Kloeden and E. Platen, *Numerical Solution of Stochastic Differential Equations*, 1st ed. (Springer-Verlag, Berlin, 1992).
- [60] S. Cesar and K. C. Huang, *FEMS Microbiol. Rev.* **41**, 672 (2017).
- [61] S. Xing, Y. Guan, and Y. Zhang, *Macromolecules* **44**, 4479 (2011).
- [62] R. R. Cheng, A. T. Hawk, and D. E. Makarov, *J. Chem. Phys.* **138**, 074112 (2013).
- [63] G. Marsaglia and T. A. Bray, *SIAM Rev.* **6**, 260 (1964).
- [64] A. Stukowski, *Modell. Simul. Mater. Sci. Eng.* **18**, 1 (2010).
- [65] M. P. Allen and D. J. Tildesley, *Computer Simulation of Liquids*, 2nd ed. (Oxford University Press, Oxford, 2017).
- [66] É. Fodor, H. Hayakawa, J. Tailleur, and F. van Wijland, *Phys. Rev. E* **98**, 062610 (2018).
- [67] J.-P. Hansen and I. R. McDonald, *Theory of Simple Liquids*, 4th ed. (Academic, Oxford, 2013).
- [68] The temperature definition of Eq. (20) and the ones in [55] differ by a factor of 2. In [55] the kinetic term is not considered because velocities are not defined in the overdamped limit. However, to fulfill our condition in the Gaussian limit, we assume that the system's kinetic and potential energy are identical (virial theorem).